LANGMUIR

Article pubs.acs.org/Langmuir

pH-Mediated Aggregation-to-Separation Transition for Colloids **Near Electrodes in Oscillatory Electric Fields**

Medha Rath, Jacqueline Weaver, Mei Wang, and Taylor Woehl*



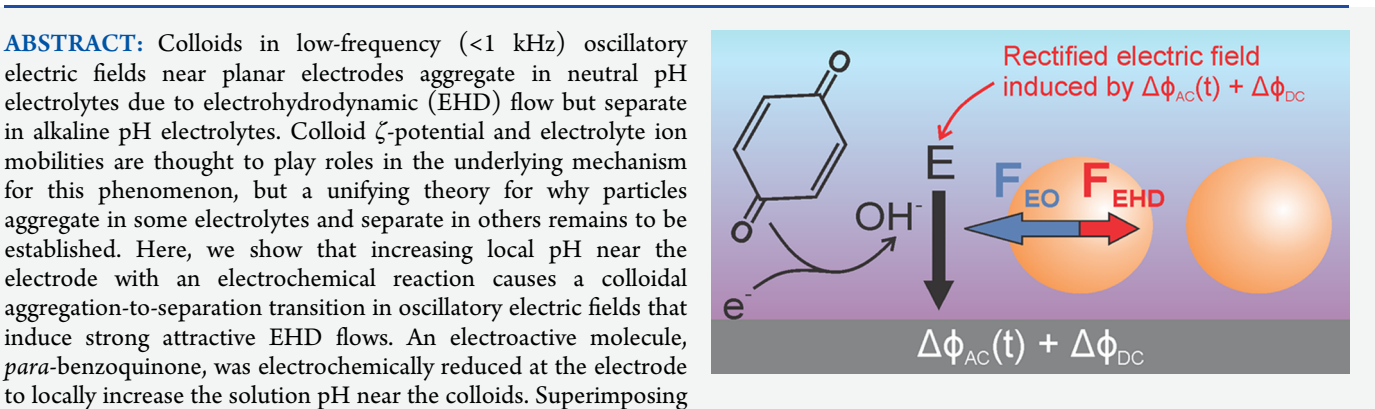
Cite This: https://doi.org/10.1021/acs.langmuir.1c00671



ACCESS

III Metrics & More

ABSTRACT: Colloids in low-frequency (<1 kHz) oscillatory electric fields near planar electrodes aggregate in neutral pH electrolytes due to electrohydrodynamic (EHD) flow but separate in alkaline pH electrolytes. Colloid ζ -potential and electrolyte ion mobilities are thought to play roles in the underlying mechanism for this phenomenon, but a unifying theory for why particles aggregate in some electrolytes and separate in others remains to be established. Here, we show that increasing local pH near the electrode with an electrochemical reaction causes a colloidal aggregation-to-separation transition in oscillatory electric fields that induce strong attractive EHD flows. An electroactive molecule, para-benzoquinone, was electrochemically reduced at the electrode



Article Recommendations

a sufficiently large steady electrochemical potential onto an oscillatory potential caused a reversible aggregation-to-separation transition. Counterintuitively, decreasing frequency, which increases attractive EHD drag forces, caused a similar aggregation-toseparation transition. Even more interesting, multiple transitions were observed while varying the oscillatory potential. Taken together, these results suggested that the oscillatory potential induced a repulsive hydrodynamic drag force. Scaling arguments for the recently discovered asymmetric rectified electric field (AREF) showed that a repulsive AREF-induced electroosmotic (EO) flow competed with attractive EHD flow. A pairwise colloidal force balance including these competing flows exhibited flow inversions qualitatively consistent with experimentally observed aggregation-to-separation transitions. Broadly, these results emphasize the importance of AREF-induced EO flows in colloid aggregation and separation in low-frequency oscillatory electric fields.

INTRODUCTION

Micron-scale dielectric colloids in dilute aqueous electrolytes (10⁻⁵ to 10⁻² M) are widely known to assemble into planar aggregates near charged electrodes in low-frequency (<1 kHz) oscillatory electric fields. 1-9 The formation of planar aggregates is attributed to attractive hydrodynamic drag forces created by electrohydrodynamic (EHD) fluid flow around each particle, which occurs due to perturbation of the otherwise spatially uniform electric field by the particles, creating a rectified electric field directed along the electrode surface that drives the EHD flow.^{2,10} In basic (NaOH) or acidic (HCl) electrolytes that induce large ζ -potentials on particles ($|\zeta_p| \sim$ 100 mV), colloids do not aggregate and in some cases separate. A large survey study found that the aggregation rate of colloids was correlated with colloid ζ -potential and electric field amplitude across 26 unique particle-electrolyte pairs.4 Recent theoretical and experimental work has shown that colloid ζ -potential, 4 surface conductivity, 19,20 and cation/anion diffusivity mismatch 17,18 play roles in whether colloids aggregate or separate in a given electrolyte. Ma et al. showed that colloids with large ζ -potential and surface conductivity generated extensile fluid flows in oscillatory fields.²⁰ Here, the

large particle surface conductivity caused the dipole moment to orient in the same direction as the applied electric field, driving an extensile EHD fluid flow. 19 However, this mechanism only explains particle separation at low ionic strengths ($\sim 10^{-5}$ M), where electrolyte conductivity is commensurate with particle surface conductivity, indicating that another mechanism must be active for higher-ionic-strength electrolytes.

Separation and aggregation of colloids in various electrolytes has previously been explained by competition between multiple extensile and contractile electrokinetic flows. 21,22 Previous work has shown that steady electric fields induce particle aggregation or separation due to electroosmotic (EO) flow along the particle surface, which creates either extensile or contractile flow around each particle depending on the sign of

Received: March 10, 2021 Revised: June 15, 2021



the steady potential and particle ζ -potential. ^{5,6,21,22} Motion of particles normal to the electrode surface also plays an important role in determining whether colloids aggregate or separate in oscillatory electric fields. 15,23 The phase angle between the oscillatory electrophoretic motion of colloids and the electric field magnitude correlates with whether particles will aggregate or separate. 11,13,14,21,24 Prior work by the Prieve group has demonstrated changes in particle height upon application of electrochemical potentials that drive water electrolysis.²⁵ In these experiments, vertical motion of the particle was effected by faradaic current density passing through the electrochemical cell. 25,26 Colloids in electrolytes where the cations and anions have different mobilities, e.g., NaOH, have been shown to separate and levitate tens of microns above the electrode surface in low-frequency oscillatory fields. ^{15,18,23} Colloid levitation was explained by the recently identified asymmetric rectified electric field (AREF), which is induced by the action of an oscillatory potential on an electrolyte with different cation and anion diffusivities.¹⁷ The disparate electrophoretic motion of ions creates free charge density outside the diffuse layer near the electrode, which partially rectifies the oscillatory current to create the AREF. 17 Recent theoretical work has suggested that AREF-induced EO flow can dominate induced charge electrokinetic flows under certain conditions, 27 but supporting experimental evidence is so far lacking.

In this article, we investigate the aggregation and separation of dielectric colloids in the presence of oscillatory electric fields and alkaline solution pH resulting from electroreduction of para-benzoquinone (BQ). Microscopic observations of colloid aggregation-to-separation transitions under various applied oscillatory potentials, frequencies, and steady electrochemical potentials were not explained alone by changes in EHD fluid flow or faradaic electric field-induced electroosmotic (EO) flow. Instead, a scaling analysis of an AREF stemming from the action of the oscillatory electric field on electrochemically generated hydroxyl ions showed that the AREF was strong enough to drive a competitive repulsive EO flow. A pairwise colloidal force balance reconciled the aggregation-to-separation transition in terms of an extensile AREF-induced EO flow around each particle that dominated contractile EHD fluid flow. This work emphasizes the importance of AREF-induced EO flow in controlling the aggregation and separation of colloids in electrolytes with unequal ion mobilities and introduces electroactive molecules as a method to probe the effects of pH and ion mobility on colloid aggregation and separation in oscillatory electric fields. Aside from fundamental electrokinetics studies, we expect electrochemical pH modifications will offer enhanced control over directed assembly of colloids into photonic structures^{28–32} and propulsion of colloidal microswimmers.^{20,33–35}

■ METHODS/EXPERIMENTAL SECTION

The experimental setup and materials are similar to those described in prior works. 4,36 Briefly, a static electrochemical cell was constructed by sandwiching two pieces of tin-doped indium oxide (ITO)-coated glass slides together separated by a $\sim\!200~\mu\mathrm{m}$ insulating spacer (Figure 1a). Electric potentials were applied using an arbitrary wave generator (AWG), with steady potentials superimposed onto oscillatory potentials by applying a constant offset potential to the oscillatory potential (Figure 1b). The AWG applied potentials to the working electrode (WE, bottom electrode) in reference to earth ground (top electrode). Silica particles were purchased from Bang's Lab and carboxylic acid-functionalized polystyrene particles were purchased

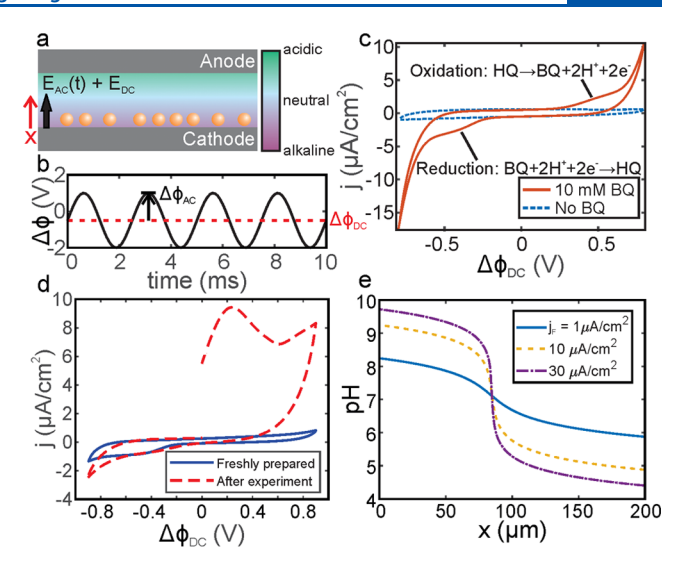


Figure 1. (a) Schematic of sample cell showing position of electrodes and the expected pH changes for a negative steady electrochemical potential. The spatial coordinate, x, used for the pH simulations is shown with the origin at the cathode surface. (b) Example waveform defining the superimposed oscillatory potential amplitude $(\Delta\phi_{\rm AC})$ and the steady potential $(\Delta\phi_{\rm DC})$. (c) Cyclic voltammogram of 10 mM BQ in 100 mM KCl (scan rate = 150 mV/s). (d) Cyclic voltammogram of 10 mM BQ in 100 mM KCl freshly prepared (blue line) and after being subjected to an oscillatory potential of 1.5 V, 400 Hz combined with a steady potential of -250 mV for 4 min (red dashed line). (e) Simulated pH for several values of faradaic current density $(j_{\rm F})$ as a function of position in the electrochemical cell. The cathode is located at the origin.

from Polysciences. The particles were prepared by dispersing in the electrolyte solution at 0.1 w/w % and centrifuging and rinsing three times to remove residual surfactants and preservatives. BQ (Sigma-Aldrich, 99.5%) solutions were prepared fresh for each experiment and kept away from light. All samples were prepared in the electrolyte of 1 mM KCl in 18.2 M Ω DI water and BQ was added to the electrolyte at a 10 mM final concentration. Video microscopy was performed on an upright optical microscope operating in bright field mode and movies were recorded using a charge-coupled device (CCD) camera. Cyclic voltammetry (CV) was performed using a Gamry Reference 600+ in a two-electrode configuration with one ITO electrode serving as the WE and the other ITO electrode serving as the counter electrode (CE) and reference electrode (RE). The electrolyte for the CV experiments was 100 mM KCl instead of 1 mM KCl to reduce the ohmic drop in the cell. Current density measurements were performed on 1 mM KCl, 10 mM BQ samples with a potentiostat operating in electrochemical impedance spectroscopy (EIS) mode by applying a mixed oscillatory and steady potential and measuring the resulting current for 30 s at each potential. Particle ζ -potentials were measured in triplicate using a Malvern Zetasizer Nano ZS90. KOH (1 mM) was used to modify the pH for the ζ potential measurements; electrolytes were sparged with argon for 1 h to remove dissolved CO₂ prior to pH adjustment.

■ RESULTS AND DISCUSSION

Electrochemical Reactions and pH Change. At nearneutral pH, BQ dissolved in water is electrochemically reduced to hydroquinone (HQ) at the cathode *via* consumption of two protons and two electrons, increasing the local pH. HQ is oxidized at the anode to BQ through the reverse pathway, which decreases the local pH (Figure 1a)^{37–40}

$$BQ + 2H^{+} + 2e^{-} \leftrightarrow HQ \tag{1}$$

Excess protons and hydroxyl ions diffuse away from the electrodes toward the center of the cell and recombine to form water. 41 Cyclic voltammetry of aqueous 10 mM BQ in 100 mM KCl showed reversible oxidation/reduction with a reduction potential of -300 mV and oxidation potential of +400 mV vs ITO reference (Figure 1c). We note that the redox potentials identified here were subject to drift in the CE/RE and may not be the true redox potentials due to the twoelectrode setup. Despite this, the CV demonstrates the important feature of the BQ/HQ couple, which is that it undergoes redox reactions within the electrochemical window of water. To further confirm that the electrochemical reaction was occurring during colloidal aggregation experiments, we subjected an electrochemical sample cell to a -250 mV steady potential superimposed on an oscillatory potential of 1.5 V, 400 Hz. After 5 min of polarization, the sample was immediately transferred to a potentiostat and electrodes connected in the same polarity as in the AWG (bottom electrode as the WE, top as the CE/RE). Compared to a CV of the sample prior to applying the mixed oscillatory and steady potential, which only showed current due to BQ reduction, the first CV cycle taken after the experiment showed a large oxidative current due to oxidation of HQ that was formed near the cathode (Figure 1d). This indicates that steady potentials less than the redox potential observed by CV can stimulate the electrochemical reaction. This may occur because the AWG applies potentials in reference to a different ground than for the CV experiments. Regardless of the underlying reason, the CV measurements confirmed that BQ/HQ redox reactions occurred during the colloidal aggregation experiments.

The pH in the sample cell was estimated by numerically solving a simplified version of the Poisson-Nernst-Planck (PNP) equations. The rate constants for the BQ/HQ reactions are unknown, so we approximated the electrochemical reactions by considering the generation and consumption of protons and hydroxyl ions at each electrode and their recombination into water with known rate constants. While this approach does not explicitly consider the BQ, HQ, or any intermediate species, it provides an estimate of the solution pH as a function of the current density to be used in a scaling model. Prior work has shown the colloids are located outside of the diffuse layer at the electrode surface, 1,15 so the numerical model did not consider electric field enhancement in the electric double layer. The PNP equations reduce to the diffusion equation under these conditions due to the absence of free charge density in the electrolyte. 42 The equilibrium reaction of protons and hydroxyl ions to form water were considered, resulting in the one-dimensional (1D) timedependent reaction-diffusion equations for protons and hydroxyl ions

$$\frac{\partial c_{H^{+}}}{\partial t} = D_{H^{+}} \frac{\delta^{2} c_{H^{+}}}{\delta x^{2}} - k_{1} c_{H^{+}} c_{OH^{-}} + k_{2} c_{H_{2}O}$$
(2)

$$\frac{\partial c_{\text{OH}^{-}}}{\partial t} = D_{\text{OH}} - \frac{\delta^{2} c_{\text{OH}^{-}}}{\delta x^{2}} - k_{1} c_{\text{H}^{+}} c_{\text{OH}^{-}} + k_{2} c_{\text{H}_{2}\text{O}}$$
(3)

Here, c_{H^+} is the concentration of protons, $D_{\text{H}^+} = 9.3 \times 10^{-9} \, \text{m}^2/\text{s}$ is the diffusion coefficient of protons in pure water, c_{OH^-} is the concentration of hydroxyl ions, $D_{\text{OH}^-} = 5.5 \times 10^{-9} \, \text{m}^2/\text{s}$ is the diffusion coefficient of hydroxyl ions in pure water, $k_1 = 1.4 \times 10^{11} \, \text{M/s}$ and $k_2 = 0.0014 \, \text{s}^{-1}$ are, respectively, the forward and back reaction rates for the equilibrium reaction of protons

and hydroxyl ions to form water, $OH^- + H^+ \rightleftharpoons \frac{k_1}{k_2} H_2O$, t is time, and x is the spatial coordinate defined in Figure 1a. Water was assumed to have a constant concentration of $c_{\rm H_2O} = 55$ M. COMSOL was used to solve this set of partial differential equations for two electrodes separated by 200 μ m. Constant flux boundary conditions were applied at each electrode to simulate generation and consumption of protons by BQ/HQ redox reactions and recombination/dissociation of w a t e r , v i z . ,

 $J_{\rm H^+,anode}$ ($x=200~\mu{\rm m}$) = $-J_{\rm H^+,cathode}$ ($x=0~\mu{\rm m}$) = $\frac{J_{\rm F}}{F}$, where $j_{\rm F}$ is the faradaic current density and F is Faraday's constant. Simulations showed the pH distribution in the cell reached steady state within a few seconds. Figure 1e shows the steady-state pH in the cell for various values of current density and shows the pH can reach alkaline values near 10 at the cathode and acidic values near 4 for a reasonable current density of 30 $\mu{\rm A/cm^2}$. The pH was relatively constant in the region containing the colloids and decayed to neutral pH near the center of the cell. These simulations did not include the equilibrium between protons and BQ or other intermediate species and are thus expected to overestimate the pH for a given current density, but the trends are expected to be internally consistent and give reasonable estimates.

Aggregation and Separation of Colloids with Electroactive Molecules. Monodisperse 3 μ m polystyrene microspheres were suspended in 1 mM KCl with 10 mM BQ added and allowed to settle to the bottom electrode by gravity where they remained colloidally stable. The particles were aggregated into two-dimensional (2D) hexagonally close-packed aggregates by applying an oscillatory potential of 2 V, 400 Hz (Figure 2a). Increasingly negative steady potentials were superimposed stepwise onto the oscillatory potential at a rate of -50 mV per 20 s and video microscopy recorded the dynamics (Figure 2b,c). The mean center-to-center interparticle separation, $\langle S \rangle$, was measured as a function of time and steady potential using Delaunay triangulation to determine the average nearest-neighbor interparticle distance (Figure 2d). The bond orientation order parameter, a measure of how hexagonally close packed the particles were, was determined by

$$\Psi_6 = 1/N \sum_{i} \left[\left| (1/N_{ij}) \sum_{j} \exp(i \ 6\theta_{ij}) \right| \right]$$
(4)

where θ_{ii} is the angle between a fixed axis and the bond separating nearest-neighbor particles i and j. An order parameter of $\Psi_6 = 1$ is a perfect hexagonally close-packed lattice while 0 is a random arrangement of particles. With only an oscillatory potential applied, the interparticle separation of the colloids was slightly larger than the particle diameter and the order parameter was ~ 0.8 (Figure 2a,d). Stepwise changes to steady potential in the range of 0 to -100 mV had no effect on the interparticle separation or order parameter. The interparticle separation of the colloids increased and the bond order parameter decreased over about 10 s to new steady-state values after a stepwise increase of steady potential to -150 mV (Figure 2b). Increasing steady potential to -200mV caused a further increase in the interparticle separation to ~1.7 particle diameters and decreased the bond order parameter to ~0.4 (Figure 2c). The colloids isotropically separated after applying a -250 mV steady potential as indicated by a monotonically increasing interparticle separation

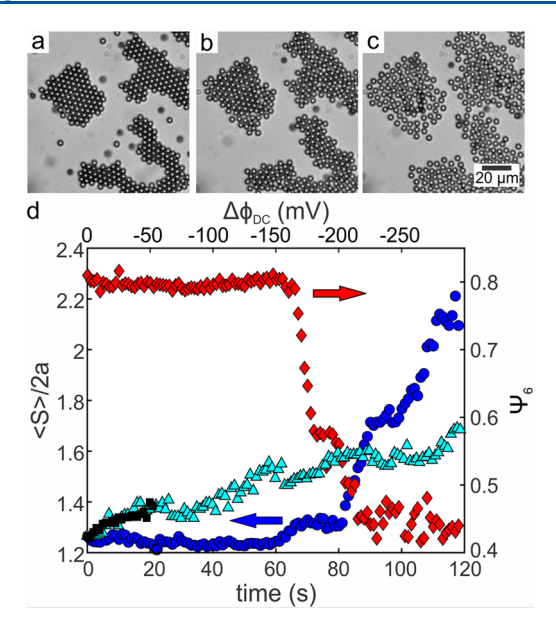


Figure 2. Aggregation-to-separation transition induced by superposition of a steady and oscillatory potential. (a–c) Images of 3 μm polystyrene colloids with different steady potentials of (a) 0 mV, (b) -150 mV, and (c) -200 mV superimposed onto a 2 V, 400 Hz oscillatory potential. (d) Average center-to-center interparticle separation normalized to the particle diameter, $\langle S \rangle/2a$, and orientational bond order parameter, Ψ_6 , of a particle aggregate as a function of time and steady potential. The steady potential was modified stepwise every 20 s. The black squares show $\langle S \rangle/2a$ of aggregated colloids separating only by Brownian motion after removing a 2 V, 400 Hz oscillatory potential. The teal triangles show $\langle S \rangle/2a$ of aggregated colloids separating under stepwise increased steady potentials with no oscillatory potential.

over time. The particles separated more quickly during the aggregation-to-separation transition compared to when particle aggregates separated by diffusion after removing an oscillatory electric field (black squares, Figure 2d), indicating a long-ranged repulsive force pushed particles apart during the transition. Particles initially aggregated in an oscillatory potential and then subjected to stepwise increases in steady potential (with no superimposed oscillatory potential) separated at a nearly identical rate to those separating by diffusion only (cyan triangles, Figure 2d). The aggregation-to-separation transition was not observed for positive steady

potentials or in the absence of BQ in the electrolyte and occurred for both polystyrene and silica microspheres. This indicates the transition only occurred at the electrode where BQ electroreduction increased pH. Colloids formed 2D aggregates upon removing the superimposed steady potential, indicating that the transition was reversible.

The critical steady potential $(\Delta\phi_{
m DC,crit})$ for the aggregationto-separation transition depended on the oscillatory potential and frequency (Figure 3). The critical steady potential was identified for several values of oscillatory potential and frequency by initially aggregating the colloids in a purely oscillatory field and then increasing the steady potential stepwise -50 mV every 20 s until the colloids showed monotonic separation in time (dashed vertical lines, Figure 3a). The critical steady potential decreased as the oscillatory potential was increased at a constant frequency (Figure 3b) and decreased as the frequency was decreased at a constant oscillatory potential (Figure 3c). These results suggested that increasing the oscillatory potential or decreasing the frequency at a constant steady potential (below the critical value for separation) would also induce an aggregation-to-separation transition. Indeed, colloids aggregated with an initially 1000 Hz, 2 V oscillatory potential and a superimposed -200 mV steady potential experienced increased repulsive forces as the frequency was decreased in 200 Hz increments every 20 s (Figure 4a-c). At a critical frequency of 400 Hz, the colloids separated entirely (Figure 4d). Separation at low frequency was accompanied by a change in the particle height above the electrode, indicated by the change in the particle contrast in Figure 4c compared to Figure 4a,b. Colloids initially aggregated in a 400 Hz, 4.5 V oscillatory potential with a constant -150 mV steady potential applied (Figure 4e) experienced increased repulsion as the oscillatory potential was decreased stepwise to 2.5 V, where they separated (Figure 4f). Intriguingly, further decreasing the oscillatory potential below 2 V caused the particles to undergo a separation to aggregation transition (Figure 4g). The two transitions are illustrated clearly in quantitative measurements of the mean interparticle separation and order parameter (Figure 4h). These results were surprising and counterintuitive considering that the magnitude of the attractive EHD fluid flow changes monotonically with oscillatory potential.¹⁰

Scaling Analysis for Aggregation-to-Separation Transition. Several mechanisms were considered to explain why

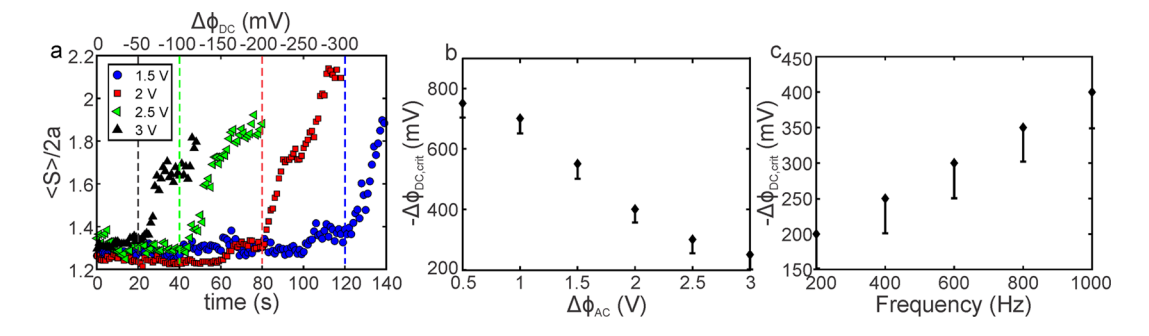


Figure 3. Effect of oscillatory potential and frequency on the critical steady potential ($\Delta\phi_{DC,crit}$) to induce the aggregation-to-separation transition in 3 μ m diameter polystyrene particles (a) and 4 μ m silica particles (b, c). (a) Mean interparticle separation normalized to particle diameter, $\langle S \rangle / 2a$, of an aggregate as a function of time and steady potential (modified stepwise every 20 s). The frequency was held constant at 400 Hz, and the steady potential was decreased by -50 mV every 20 s. The colored dashed lines indicate the critical steady potentials for inducing separation. (b, c) Effect of the oscillatory potential (b) and frequency (c) on the critical steady potential. The black diamonds indicate the identified value, while the error bars indicate the possible range for each condition. The frequency in (b) was 400 Hz, and the oscillatory potential in (c) was 1 V.

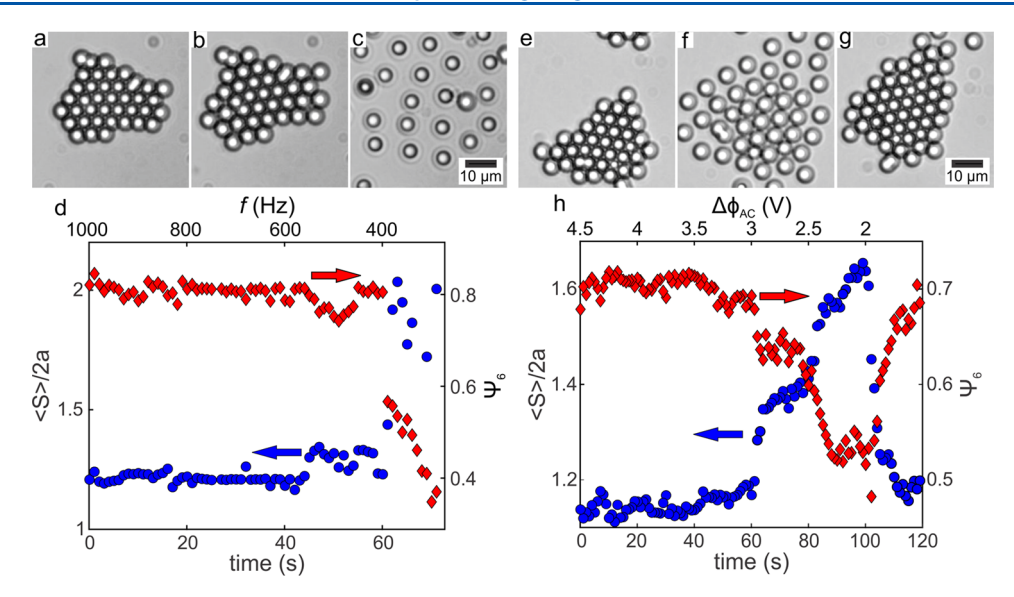


Figure 4. Decreasing frequency at constant steady potential caused an aggregation-to-separation transition, while multiple transitions were observed when varying oscillatory potential. (a–c) Images of 4 μ m silica colloids at different frequencies of (a) 800 Hz, (b) 600 Hz, and (c) 400 Hz. The oscillatory potential was 2 V, the steady potential was –150 mV, and the frequency was decreased stepwise every 20 s. (d) Average interparticle separation normalized to particle diameter, $\langle S \rangle/2a$, and orientational bond order parameter, Ψ_6 , of a particle aggregate as a function of time and frequency. (e–g) Images of 4 μ m silica colloids at different oscillatory potentials of (e) 4.5 V, (f) 2.5 V, and (g) 2 V. The frequency was 400 Hz, the steady potential was –150 mV, and the oscillatory potential was decreased stepwise every 20 s. (h) Average interparticle separation normalized to particle diameter, $\langle S \rangle/2a$, and orientational bond order parameter, Ψ_6 , of a particle aggregate as a function of time and oscillatory voltage.

particles separate when a steady potential was superimposed onto an oscillatory potential. Qualitative experimental observations provided preliminary insights. First, repulsive interparticle forces that caused the aggregation-to-separation transition were long-ranged and acted over several particle diameters to separate particles at a faster rate than diffusion. This rules out colloidal electrostatic interactions that act over particle separations of hundreds of nanometers; specifically, pH increases near the cathode increasing particle ζ -potential and electrostatic repulsion cannot cause long-ranged repulsion. Dipole-dipole repulsion forces are not expected to be significantly affected by changes to pH, steady potential, or frequency, indicating they likely do not cause the aggregationto-separation transition. Dipole-dipole forces scale quadratically with oscillatory potential and would not lead to a separation to aggregation transition with decreasing oscillatory potential. Immediately prior to an aggregation-to-separation transition, the interparticle separation increased to a larger steady-state value (cf. Figures 2d and 4d). Together with the observations of long-ranged repulsion, this observation suggests that separation of colloids was mediated by a balance between attractive and repulsive hydrodynamic drag forces. Specifically, we hypothesize that a steady electric field resulting from the electrochemical reaction drives a repulsive EO flow on the particle surface that directly opposes attractive EHD drag forces. For a negatively charged particle and electric field pointing toward the bottom electrode, the EO flow is directed toward the electrode and creates repulsive drag forces between neighboring particles.²²

First, we consider whether the faradaic electric field $(E_{\rm F})$ created by the electrochemical redox reactions induces the repulsive EO flow. The extensile EO flow along the particle surface scales as

$$U_{\rm EO} \sim \frac{\in \in_0 \zeta_{\rm p} E_{\rm F}}{\mu} \tag{5}$$

where $U_{\rm EO}$ is the EO flow magnitude, $\epsilon\epsilon_0$ is the relative permittivity, $\zeta_{\rm P}$ is the particle ζ -potential, μ is the solution viscosity, and $E_{\rm F}=\frac{j_{\rm F}}{\sigma}$, where σ is the electrolyte conductivity. Reasonable estimates for the Faradaic current density of 10 $\mu{\rm A/cm^2}$ and particle ζ -potential of -40 mV yield a faradaic electric field magnitude of 5 V/m and an EO flow magnitude of $U_{\rm EO}\sim 10^{-1}~\mu{\rm m/s}$. Prior estimates and measurements of EHD fluid flows are in the range of $1-10^2~\mu{\rm m/s}$, 10,20 indicating that the faradaic electric field-induced EO flow is likely too weak to overcome the attractive EHD fluid flow and cause particle separation. Experimental observations showing that particles did not separate faster than by diffusion when only a negative steady electrochemical potential was applied support this assertion (Figure 2d).

Another possible explanation for the transition is the local increase in solution pH and particle ζ -potential decreases the particle dipole field strength, which decreases the EHD flow magnitude. To test whether this mechanism explains the particle separation, we performed a scaling analysis of the pH and ζ -potential dependence of the EHD fluid flow (see Table 1

Table 1. Summary of Parameters for EHD Flow Scaling Model

relative permittivity of water (ϵ)	80
diffusion coefficient (D)	$2.05 \times 10^{-9} \text{ m}^2/\text{s}$
Debye length (κ^{-1})	9.7 nm
electrode spacing (l)	200 μm
temperature (T)	298 K
viscosity of water (μ)	0.894 mPa·s
particle radius (a)	$2 \mu m$

for model parameters). The EHD flow magnitude ($U_{\rm EHD}$) can be estimated by the following scaling expression 10

$$U_{\text{EHD}} \approx K_0 \frac{3 \in \epsilon_0}{2\mu\kappa} \left(\frac{\Delta\phi_{\text{AC}}}{l}\right)^2 \left\{ C_0' \left(1 + \frac{\kappa^3 D^2}{\omega^2 l}\right) + C_0'' \frac{\kappa^2 D}{\omega} \right\}$$
(6)

Here, $K_0 = 0.02$ is a fitting parameter determined from a previous work, 33 κ is the Debye parameter, C_0' and C_0'' are the real and imaginary parts of the particle dipole coefficient, respectively, ω is the angular frequency, and D is the average ion diffusion coefficient. The particle dipole coefficient ($C_0 = C_0' + iC_0''$) quantifies the direction/magnitude (C_0') and phase (C_0'') of the particle polarization and is a function of the particle radius, ζ -potential, Debye length, ion mobilities, and electric field frequency. 43 To determine how the EHD flow magnitude changes with pH and current density, we experimentally measured the ζ -potential of 4 μ m diameter silica spheres as a function of pH (Figure 5a). Based on the

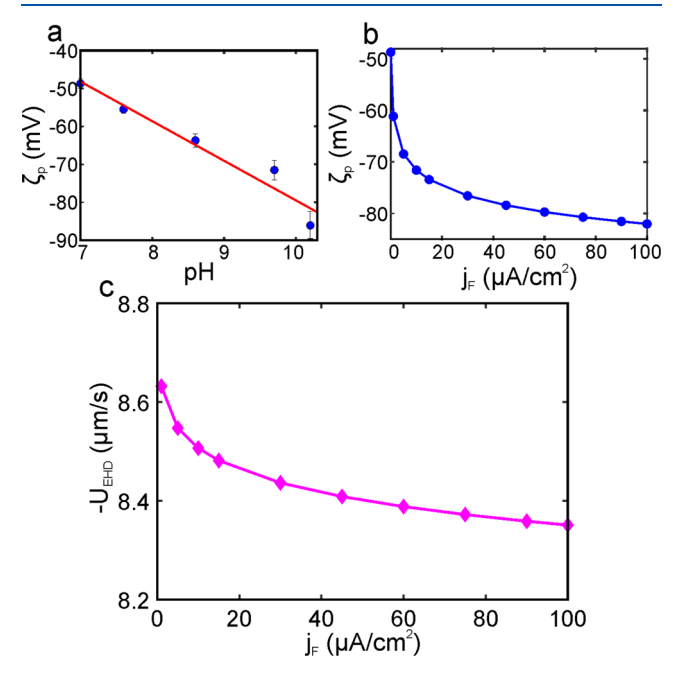


Figure 5. (a) ζ-Potential of 4 μ m diameter silica as a function of pH in 1 mM KCl. (b) Estimated ζ-potential of silica particles located 1 μ m from the cathode as a function of faradaic current density. (c) EHD fluid flow velocity as a function of faradaic current density. The oscillatory potential was 0.5 V, and the frequency was 400 Hz.

numerical pH simulations (cf. Figure 1d) the pH 1 μ m from the cathode was determined as a function of the current density. Together the pH simulations and experimental ζ -potentials provided an estimate of the current density-dependent particle ζ -potential (Figure 5b). The dipole coefficient was calculated from the low-frequency asymptotic solution to the standard electrokinetic model solved by Shilov et al. ^{19,43} Despite the ζ -potential increasing by a factor of 2 when increasing the current density from 0 to 100 μ A/cm², the EHD flow magnitude decreased by less than 10% (Figure 5c). This is because corresponding increases to the particle surface conductivity were small compared to the bulk electrolyte conductivity, resulting in minor decreases in the particle dipole field strength. This analysis indicates that the EHD drag force will remain attractive under all conditions here and the

electrochemical reactions will not significantly affect the EHD flow magnitude.

Understanding can be gleaned by considering a pairwise colloidal force balance including opposing hydrodynamic drag forces on the particles: one due to contractile EHD flow (attractive drag force) and the other an extensile faradaic electric field-induced EO flow (repulsive drag force). The force balance is formulated in terms of the relative velocity of the particle pair $(U_{\rm relative})$

$$U_{\text{relative}} = -2(U_{\text{EHD}} + U_{\text{EO}}) \tag{7}$$

Here, a positive relative velocity corresponds to net attraction between the particles while a negative velocity signifies net repulsion. The critical current density ($j_{\rm crit} \propto \Delta\phi_{\rm DC,crit}$) required to induce an aggregation-to-separation transition can be obtained by setting $U_{\rm relative}=0$. Considering only terms expected to vary with oscillatory and steady potential for each flow term, viz., $U_{\rm EHD} \sim \frac{\Delta\phi_{\rm AC}^2}{f}$ and $U_{\rm EO} \sim j$, yields a scaling expression for the critical current density for particle separation, $j_{\rm crit} \sim \frac{\Delta\phi_{\rm AC}^2}{f}$. Based on this balance, increasing the oscillatory potential or decreasing the frequency should increase the critical steady-state potential required to separate particles. However, our observations of the opposite trend (cf. Figure 4) indicate this force balance is not correct. More precisely, the experiments suggest the oscillatory electric field induces repulsive drag forces between particles that are a function of frequency and oscillatory potential.

The recently discovered AREF is a steady electric field induced by applying an oscillatory potential to an aqueous electrolyte with mismatched ion mobilities, such as millimolar KOH.¹⁷ When an oscillatory potential is applied to the electrolyte, the different electrophoretic mobilities of the cations and anions lead to a nonzero, time-independent free charge density and steady electric field in the liquid. The ion mobility mismatch is quantified by $\delta = \frac{D_-}{D_+}$, where D_- and D_+ are the anion and cation diffusivities.⁴⁴ Prior work has investigated AREF in electrolytes with a permanent mismatch in ion diffusivity, e.g., aqueous NaOH and KOH.17,18 In the present experiments, electroreduction of BQ at the cathode consumes protons and increases the local hydroxyl ion concentration due to water dissociation, which creates a local ion diffusivity mismatch. The increased hydroxyl ion concentration at the bottom electrode leads to $\delta > 1$ due to the larger diffusion coefficient of hydroxyl ions $(D_{\rm OH^-}=5.27\times 10^{-9}~m^2/s)$ compared to potassium ions $(D_{K^+} = 1.96 \times 10^{-9} \, m^2/s)$, resulting in an AREF that is oriented toward the bottom electrode where the colloids are located. Numerical pH simulations showed that steady-state hydroxyl ion concentrations can reach 1 mM near the cathode for a current density of 50 μ A/cm² (cf. Figure 1c), nearly equimolar to the potassium and chloride ion concentrations. The local value of δ in the electrolyte solution was estimated by calculating an average anion diffusivity, $D_{-,ave} = D_{OH} x_{OH} +$ $D_{CI} x_{CI}$, where the anion diffusivities are weighted by their local mole fraction (x_i) in solution. δ ranges from 1.05 to 1.3 for faradaic current densities ranging from 5 to 100 μ A/cm², which are less than half that of those for pure KOH (δ = 2.6). We applied prior scaling arguments to estimate the peak magnitude of the AREF field*

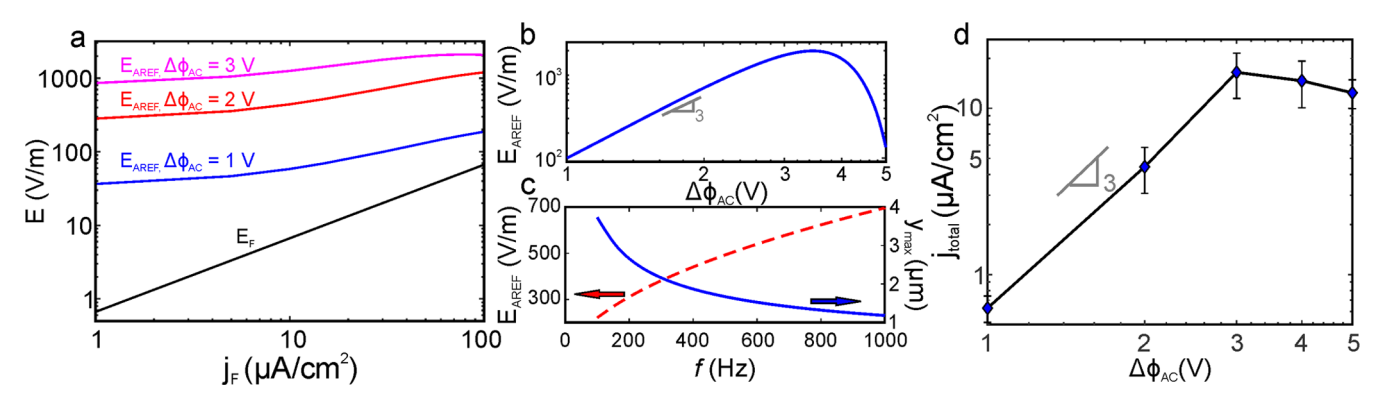


Figure 6. AREF scaling arguments and experimental AREF measurements. (a) Maximum AREF (E_{AREF}) and faradaic electric field (E_{F}) magnitudes as a function of the faradaic current density for several oscillatory potentials at a constant frequency of 400 Hz. The black line is the faradaic electric field. (b) Maximum AREF magnitude as a function of oscillatory potential for a frequency of 400 Hz. (c) Maximum AREF field magnitude and its distance from the cathode in the electrochemical cell (y_{max}) as a function of frequency for a constant oscillatory potential of 2 V and current density of 10 μ A/cm². (d) Experimental measurement of the total steady current density (j_{total}) magnitude as a function of oscillatory potential for a constant steady potential of -200 mV and a frequency of 400 Hz. Current density was measured in triplicate for each oscillatory potential, and the measurements were taken in random order to avoid any hysteresis effects.

$$E_{\text{AREF}} \approx K \Delta \phi_{\text{AC}}^3 \gamma \left(\frac{f}{D_{-,\text{ave}} D_{+} \kappa l} \right)^{1/2} \left(\frac{e}{k_{\text{B}} T} \right)^2$$
 (8)

$$\gamma = \alpha \, \exp\left(-\frac{|\alpha|}{\alpha_{\text{max}}}\right) \tag{9}$$

$$\alpha = \frac{(D_{-,ave} - D_{+})}{\sqrt{D_{-,ave}D_{+}}}$$
(10)

$$\alpha_{\text{max}} = \delta_{\text{max}} - \frac{1}{\sqrt{\delta_{\text{max}}}} \tag{11}$$

$$\delta_{\text{max}} = k_1 - k_2 \frac{\exp\left(\frac{k_3 \Delta \phi_{\text{AC}} e}{k_{\text{B}} T}\right)}{1 + \exp\left(\frac{k_3 \Delta \phi_{\text{AC}} e}{k_{\text{B}} T}\right)}$$
(12)

Here, $E_{\rm AREF}$ is the peak AREF magnitude; $K = 2.1 \times 10^{-4}$ m/s^{1/2}; $k_1 = 9.5$, $k_2 = 8.5$, and $k_3 = 0.03$ are fitting parameters; f is the frequency; l is the electrode separation; e is the elementary charge; $k_{\rm B}$ is the Boltzmann constant; and T is the temperature.⁴⁴ The maximum AREF magnitude is within 10 μ m of the electrode with the position dependent on the frequency, electrode separation, and ion diffusivities

$$y_{\text{max}} \approx \frac{K_1}{l} \left(\frac{D_{-,\text{ave}} D_+}{f} \right)^{1/2} \tag{13}$$

where $K_1 = 0.83$ m/s^{1/2} is a fitting parameter. ⁴⁴ The five fitting parameters were obtained in a previous study by fitting scaling expressions to full numerical simulations. ⁴⁴ Figure 6a shows that the maximum AREF magnitude increases as a function of faradaic current density with a variable, sublinear power law due to the increase in the hydroxyl ion concentration and δ near the cathode. Over the expected range of experimental current densities of $10-100~\mu\text{A/cm}^2$, the AREF magnitude scales approximately as $E_{\text{AREF}} \sim j_{\text{F}}^{1/2}$. The maximum AREF magnitude was always predicted to be larger than the faradaic electric field over the range of current densities, oscillatory potentials, and frequencies used in the experiments. The AREF magnitude scales as the oscillatory potential cubed (Figure 6b)

for oscillatory potentials <3 V and above this potential the AREF magnitude decreases because large amplitude oscillations of hydroxyl ions drive them into the electric double layers, decreasing the ion diffusivity mismatch.⁴⁴ The AREF magnitude increases as the square root of frequency across the entire range tested (Figure 6c) and the position of the maximum AREF field strength was several microns from the cathode and decreased with frequency (Figure 6c).

The total current density flowing through an electrochemical cell was measured with a potentiostat as a function of the oscillatory potential for a constant steady potential of -200mV and frequency of 400 Hz (Figure 6d). The total current density increased with a cubic power law dependence on the oscillatory potential amplitude up to 3 V, after which the current density decreased with increasing potential, which supports the presence of an AREF-induced current. The oscillatory potential corresponding to the peak current density was similar to that of the AREF scaling model (3.5 V), but the current density did not decrease above this potential as significantly as predicted by the AREF model (Figure 6b). This difference may be due to the presence of electrochemical reactions or limitations of the AREF scaling model. Despite this difference, this initial experimental evidence supports the existence of AREF here as the dominant steady electric field as opposed to the faradaic electric field, which would show a monotonic increase in current density with potential.

Lateral Force Balance. With expressions in hand for EHD flow and AREF, we computed a force balance between two particles where an AREF field-induced repulsive EO flow opposes an attractive EHD fluid flow.²⁷ Only fitting parameters previously calculated in other studies were used when computing the force balance; no free parameters were involved in the model. The scaling calculations above estimate that the AREF was at least an order of magnitude larger than the faradaic electric field, suggesting that AREF-induced EO flow will directly compete with EHD fluid flow. We calculated the force balance for two 4 μ m diameter particles separated by one particle radius and located 1 μ m from the cathode surface (eq 7). We present results as a function of the faradaic current density because this was used to parameterize the numerical model for pH calculations. The EHD fluid flow was relatively constant with faradaic current density, while the EO flow

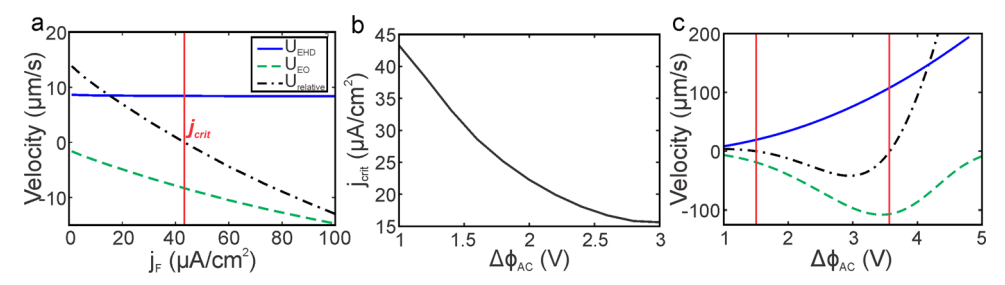


Figure 7. Lateral force balance including attractive EHD flow and repulsive AREF-induced EO flow. (a) EO flow, EHD flow, and relative pair velocity for a frequency of 400 Hz and oscillatory potential of 1 V as a function of faradaic current density. The red vertical line shows the critical faradaic current density (j_{crit}) at which flow inverts from attractive to repulsive. (b) Critical current density for an attractive to repulsive flow inversion decreases with increasing oscillatory potential. The frequency was 400 Hz. (c) EO flow, EHD flow, and relative pair velocity as a function of oscillatory potential for a constant current density of 30 μ A/cm² and a constant frequency of 400 Hz. The red vertical lines indicate flow direction inversions.

increased with current density due to the increase in ion diffusivity mismatch (Figure 7a). At low current densities, the EHD flow dominated, but as the current density was increased, the repulsive drag forces from the AREF-induced EO flow created a net repulsive flow (red dashed line). The critical current density required to generate a net extensile flow decreased with increasing oscillatory potential (Figure 7b), consistent with our experiments showing a smaller critical steady potential was required to separate particles at higher oscillatory potentials (cf. Figure 3). The scaling model was also consistent with results showing an aggregation-to-separation transition followed by a separation to aggregation as the oscillatory potential was decreased at a constant steady potential (Figure 7c). At high oscillatory potentials of >3.5 V, the EHD flow dominated AREF-induced EO flow, but as the oscillatory potential decreased the EO flow eventually overtook the EHD flow at about 3.5 V. Further decreases to oscillatory potential diminished the AREF-induced EO flow at a faster rate $(U_{\rm EO} \sim \Delta \phi_{\rm AC}^3)$ than the EHD fluid flow $(U_{\rm EHD} \sim$ $\Delta \phi_{\rm AC}^2$), leading to a second flow direction inversion at ~1.5 V. This trend cannot be explained by the direct effect of the oscillatory potential on the faradaic current, which would cause a monotonic increase in the EO flow with increasing oscillatory potential. The reproduction by the force balance of the complex colloidal dynamics when varying oscillatory potential provides strong evidence implicating AREF-induced EO flow as the driving force for the aggregation-to-separation transition. Experimental observations that the aggregation-to-separation transition did not occur for positive steady potentials, which yield δ < 1, γ < 0, and $\langle E \rangle_{AREF}$ > 0, further supports AREFinduced EO flow as the underlying phenomenon. Finally, experimental current measurements showing qualitatively similar dependence of total current density on oscillatory potential to the AREF model contribute additional strong evidence supporting this mechanism.

Several assumptions were made in deriving the scaling model for the force balance. First, the force balance was based on scaling arguments for the electrokinetic fluid flows that did not capture the spatial variations of the EHD and EO flows around each particle. Second, the pH model did not consider electromigration of ions or the effects of the oscillatory field on the electrochemical reaction. The pH model likely overestimated the solution pH for a given current density because it did not consider the proton equilibrium with BQ. Finally, the model utilized expressions for the AREF field derived for a purely oscillatory electric field and did not consider the impact of the steady potential on the AREF field. These simplifications

were necessary considering the complexity of the system as without them complex numerical simulations would be required. Despite these simplifications, the scaling model captured the qualitative features of the experiments and provides useful physical insights into the driving force for the transitions.

The scaling arguments above indicate the AREF and EO flow magnitudes should increase as the square root of frequency, which is seemingly at odds with experimental results showing that particle aggregates in large frequency oscillatory fields required larger critical steady potentials to induce separation (cf. Figure 3). However, this scaling analysis did not consider changes to the particle height relative to the electrode (cf. Figure 4), which are known to play an important role in aggregation and separation of colloids in oscillatory electric fields. Indeed, increases in particle height with decreasing frequency were observed in this study (cf. Figure 4c) and in several prior reports and have been attributed to AREF-induced electrophoretic lift forces. 1,15,18,23 The EHD fluid flow magnitude is sensitive to particle height, with a prior scaling argument predicting the EHD flow magnitude to vary with particle height (h) as $U_{\rm EHD} \sim h^{-4.2}$ Confocal microscopy measurements showed the particle height increased 2-fold when decreasing the frequency from 1 kHz to 100 Hz, which would result in a 16-fold decrease in the EHD flow magnitude. In comparison, the AREF-induced EO flow decreases by $\sim 30\%$ over the same frequency range. Based on these scaling estimates, we conclude that the threshold steady potential to induce particle separation decreases with frequency due to the increasing particle height at low frequencies, which diminishes the EHD fluid flow at a faster rate than the AREF-induced EO flow. Recasting the force balance scaling argument to include AREF-induced EO flow and particle height effects on the EHD flow yields $j_{\text{crit}} \sim \frac{1}{\int_{3}^{3} h^{8} \Delta \phi_{AC}^{2}}$ (for oscillatory potentials of <3 V).

The exact dependence of particle height on frequency is not known here, but a scaling of $h \sim f^{-1/2}$ based on the AREF scaling argument (eq 13) yields $j_{\rm crit} \sim \frac{f}{\Delta\phi_{\rm AC}^2}$, which qualitatively agrees with the experimentally observed increase in critical steady potential with frequency (Figure 3c) and decrease with oscillatory potential (Figure 3b). We did not consider this scaling quantitatively within the context of the colloidal force balance due to the unknown dependence of particle height on frequency, but these estimates along with prior observations of particle height changes provide strong evidence for diminished EHD flow as the mechanism for the

frequency-induced aggregation-to-separation transition. This mechanism is distinct from the oscillatory voltage- and current density-induced aggregation-to-separation transitions, which did not involve significant changes in the particle height or EHD flow magnitude.

CONCLUSIONS

We investigated the aggregation and separation of micron-scale colloids near charged electrodes in low-frequency oscillatory electric fields with electrochemically mediated pH changes. Colloids initially aggregated in oscillatory electric fields separated when sufficiently large steady cathodic electrochemical potentials were superimposed. The mechanism for colloid separation was explored by systematic experiments and scaling arguments based on a balance between attractive EHD fluid flow and repulsive EO flow. We found that an AREFdriven EO flow that directly competes with the EHD flow was broadly consistent with our experimental results. This indicates that the oscillatory potential induced both contractile and extensile fluid flows, where the AREF-induced EO flow dominated at intermediate ranges of oscillatory potentials, low frequencies, and high electrochemical potential. Increasing the steady potential caused particle separation by increasing the EO flow magnitude, while decreasing the frequency diminished the EHD flow by increasing the particle height above the electrode. The nonmonotonic dependence of AREF magnitude on oscillatory potential effected aggregation to separation to aggregation transitions when varying oscillatory potential.

Prior theoretical work has indicated that AREF-induced electrokinetic flow can dominate induced charge electrokinetics in some cases; 27 this study represents an initial experimental corroboration of this theory by showing AREF can induce separation of colloids with strong attractive EHD flows. This study provides further evidence supporting repulsive AREF-induced electrokinetic flows as the underlying mechanism for the observed electrolyte dependence of particle aggregation in low-frequency oscillatory electric fields. ⁴ Based on this work and past work in very dilute electrolytes, 19 we suggest a preliminary unifying explanation for electrolytedependent particle separation and aggregation in lowfrequency oscillatory fields. In dilute electrolytes ($\sim 10^{-5}$ M), colloid ζ -potential mediates the EHD flow magnitude, where sufficiently large particle ζ -potential causes flow inversion and particle separation. In more concentrated electrolytes such as the 1 mM KCl used here or millimolar NaOH/KOH electrolytes used in prior studies, 4,17,23 EHD flow magnitude is not significantly affected by high pH or ζ -potential and instead repulsive AREF-induced EO flow causes particle separation.

AUTHOR INFORMATION

Corresponding Author

Taylor Woehl — Department of Chemical and Biomolecular Engineering, University of Maryland, College Park, Maryland 21044, United States; ⊙ orcid.org/0000-0002-4000-8280; Email: tjwoehl@umd.edu

Authors

Medha Rath – Department of Chemistry and Biochemistry, University of Maryland, College Park, Maryland 21044, United States

I

- Jacqueline Weaver Department of Chemical and Biomolecular Engineering, University of Maryland, College Park, Maryland 21044, United States
- Mei Wang Department of Chemical and Biomolecular Engineering, University of Maryland, College Park, Maryland 21044, United States

Complete contact information is available at: https://pubs.acs.org/10.1021/acs.langmuir.1c00671

Notes

The authors declare no competing financial interest.

ACKNOWLEDGMENTS

The authors acknowledge financial support for this work from the National Science Foundation under grant NSF-CBET-2025249.

REFERENCES

- (1) Dutcher, C. S.; Woehl, T. J.; Talken, N. H.; Ristenpart, W. D. Hexatic-to-Disorder Transition in Colloidal Crystals Near Electrodes: Rapid Annealing of Polycrystalline Domains. *Phys. Rev. Lett.* **2013**, *111*, No. 128302.
- (2) Ristenpart, W. D.; Aksay, I. A.; Saville, D. A. Assembly of colloidal aggregates by electrohydrodynamic flow: Kinetic experiments and scaling analysis. *Phys. Rev. E* **2004**, *69*, No. 021405.
- (3) Prieve, D. C.; Sides, P. J.; Wirth, C. L. 2-D assembly of colloidal particles on a planar electrode. *Curr. Opin. Colloid Interface Sci.* **2010**, *15*, 160–174.
- (4) Woehl, T. J.; Heatley, K. L.; Dutcher, C. S.; Talken, N. H.; Ristenpart, W. D. Electrolyte-Dependent Aggregation of Colloidal Particles near Electrodes in Oscillatory Electric Fields. *Langmuir* **2014**, *30*, 4887–4894.
- (5) Bohmer, M. In situ observation of 2-dimensional clustering during electrophoretic deposition. *Langmuir* **1996**, *12*, 5747–5750.
- (6) Solomentsev, Y.; Bohmer, M.; Anderson, J. L. Particle clustering and pattern formation during electrophoretic deposition: A hydrodynamic model. *Langmuir* 1997, 13, 6058–6068.
- (7) Giersig, M.; Mulvaney, P. Formation of Ordered 2-Dimensional Gold Colloid Lattices By Electrophoretic Deposition. *J. Phys. Chem. A* **1993**, 97, 6334–6336.
- (8) Yan, J.; Rashidi, A.; Wirth, C. L. Single and ensemble response of colloidal ellipsoids to a nearby ac electrode. *Colloids Surf., A* **2020**, 606. No. 125384.
- (9) Trau, M.; Saville, D. A.; Aksay, I. A. Field-induced layering of colloidal crystals. *Science* **1996**, *272*, 706–709.
- (10) Ristenpart, W. D.; Aksay, I. A.; Saville, D. A. Electrohydrodynamic flow around a colloidal particle near an electrode with an oscillating potential. *J. Fluid Mech.* **2007**, *575*, 83–109.
- (11) Hoggard, J. D.; Sides, P. J.; Prieve, D. C. Electrolyte-dependent pairwise particle motion near electrodes at frequencies below 1 kHz. *Langmuir* **2007**, 23, 6983–6990.
- (12) Hoggard, J. D.; Sides, P. J.; Prieve, D. C. Electrolyte-dependent multiparticle motion near electrodes in oscillating electric fields. *Langmuir* **2008**, *24*, 2977–2982.
- (13) Wirth, C. L.; Rock, R. M.; Sides, P. J.; Prieve, D. C. Single and Pairwise Motion of Particles near an Ideally Polarizable Electrode. *Langmuir* **2011**, *27*, 9781–9791.
- (14) Wirth, C. L.; Sides, P. J.; Prieve, D. C. Electrolyte dependence of particle motion near an electrode during ac polarization. *Phys. Rev. E* **2013**, 87, No. 032302.
- (15) Woehl, T. J.; Chen, B. J.; Heatley, K. L.; Talken, N. H.; Bukosky, S. C.; Dutcher, C. S.; Ristenpart, W. D. Bifurcation in the Steady-State Height of Colloidal Particles near an Electrode in Oscillatory Electric Fields: Evidence for a Tertiary Potential Minimum. *Phys. Rev. E* 2015, 5, No. 011023.

- (16) Saini, S.; Bukosky, S. C.; Ristenpart, W. D. Influence of Electrolyte Concentration on the Aggregation of Colloidal Particles near Electrodes in Oscillatory Fields. *Langmuir* **2016**, *32*, 4210–4216.
- (17) Amrei, S.; Bukosky, S. C.; Rader, S. P.; Ristenpart, W. D.; Miller, G. H. Oscillating Electric Fields in Liquids Create a Long-Range Steady Field. *Phys. Rev. Lett.* **2018**, *121*, No. 185504.
- (18) Bukosky, S. C.; Amrei, S.; Rader, S. P.; Mora, J.; Miller, G. H.; Ristenpart, W. D. Extreme Levitation of Colloidal Particles in Response to Oscillatory Electric Fields. *Langmuir* **2019**, *35*, 6971–6980.
- (19) Yang, X.; Johnson, S.; Wu, N. The Impact of Stern-Layer Conductivity on the Electrohydrodynamic Flow Around Colloidal Motors under an Alternating Current Electric Field. *Adv. Intell. Syst.* **2019**, *1*, No. 1900096.
- (20) Ma, F. D.; Yang, X. F.; Zhao, H.; Wu, N. Inducing Propulsion of Colloidal Dimers by Breaking the Symmetry in Electrohydrodynamic Flow. *Phys. Rev. Lett.* **2015**, *115*, No. 208302.
- (21) Fagan, J. A.; Sides, P. J.; Prieve, D. C. Mechanism of rectified lateral motion of particles near electrodes in alternating electric fields below 1 kHz. *Langmuir* **2006**, 22, 9846–9852.
- (22) Ristenpart, W. D.; Aksay, I. A.; Saville, D. A. Electrically Driven Flow near a Colloidal Particle Close to an Electrode with a Faradaic Current. *Langmuir* **2007**, *23*, 4071–4080.
- (23) Bukosky, S. C.; Ristenpart, W. D. Simultaneous Aggregation and Height Bifurcation of Colloidal Particles near Electrodes in Oscillatory Electric Fields. *Langmuir* **2015**, *31*, 9742–9747.
- (24) Rock, R. M.; Sides, P. J.; Prieve, D. C. The effect of electrode kinetics on electrophoretic forces. *J. Colloid Interface Sci.* **2013**, 393, 306–313.
- (25) Wirth, C. L.; Sides, P. J.; Prieve, D. C. The imaging ammeter. J. Colloid Interface Sci. 2011, 357, 1–12.
- (26) Rock, R. M.; Sides, P. J.; Prieve, D. C. Ensemble average TIRM for imaging amperometry. *J. Colloid Interface Sci.* **2013**, 403, 142–150.
- (27) Amrei, S.; Miller, G. H.; Ristenpart, W. D. Asymmetric rectified electric fields generate flows that can dominate induced-charge electrokinetics. *Phys. Rev. Fluids* **2020**, *5*, No. 013702.
- (28) Gong, J.; Wu, N. Electric-Field Assisted Assembly of Colloidal Particles into Ordered Nonclose-Packed Arrays. *Langmuir* **2017**, 33, 5769–5776.
- (29) Ma, F.; Wu, D. T.; Wu, N. Formation of Colloidal Molecules Induced by Alternating-Current Electric Fields. *J. Am. Chem. Soc.* **2013**, 135, 7839–7842.
- (30) He, M.; Gales, J. P.; Ducrot, É.; Gong, Z.; Yi, G.-R.; Sacanna, S.; Pine, D. J. Colloidal diamond. *Nature* **2020**, *585*, 524–529.
- (31) Chen, Q.; Bae, S. C.; Granick, S. Directed self-assembly of a colloidal kagome lattice. *Nature* **2011**, *469*, 381–384.
- (32) Rao, A. B.; Shaw, J.; Neophytou, A.; Morphew, D.; Sciortino, F.; Johnston, R. L.; Chakrabarti, D. Leveraging Hierarchical Self-Assembly Pathways for Realizing Colloidal Photonic Crystals. *ACS Nano* **2020**, *14*, 5348–5359.
- (33) Ma, F. D.; Wang, S. J.; Wu, D. T.; Wu, N. Electric-field-induced assembly and propulsion of chiral colloidal clusters. *Proc. Natl. Acad. Sci. U.S.A.* **2015**, *112*, 6307–6312.
- (34) Ohiri, U.; Shields, C. W.; Han, K.; Tyler, T.; Velev, O. D.; Jokerst, N. Reconfigurable engineered motile semiconductor microparticles. *Nat. Commun.* **2018**, *9*, No. 1791.
- (35) Wang, Z.; Wang, Z.; Li, J.; Tian, C.; Wang, Y. Active colloidal molecules assembled via selective and directional bonds. *Nat. Commun.* **2020**, *11*, No. 2670.
- (36) Ferrick, A.; Wang, M.; Woehl, T. J. Direct Visualization of Planar Assembly of Plasmonic Nanoparticles Adjacent to Electrodes in Oscillatory Electric Fields. *Langmuir* **2018**, *34*, 6237–6248.
- (37) Quan, M.; Sanchez, D.; Wasylkiw, M. F.; Smith, D. K. Voltammetry of quinones in unbuffered aqueous solution: Reassessing the roles of proton transfer and hydrogen bonding in the aqueous Electrochemistry of Quinones. *J. Am. Chem. Soc.* **2007**, *129*, 12847–12856.
- (38) Baxendale, J. H.; Hardy, H. R. The Ionization Constants Of Some Hydroquinones. *Trans. Faraday Soc.* **1953**, *49*, 1140–1144.

- (39) Bailey, S. I.; Ritchie, I. M. A Cyclic Voltammetric Study Of The Aqueous Electrochemistry Of Some Quinones. *Electrochim. Acta* 1985, 30, 3–12.
- (40) Fomina, N.; Johnson, C. A.; Maruniak, A.; Bahrampour, S.; Lang, C.; Davis, R. W.; Kavusi, S.; Ahmad, H. An electrochemical platform for localized pH control on demand. *Lab Chip* **2016**, *16*, 2236–2244
- (41) Balakrishnan, D.; Lamblin, G.; Thomann, J. S.; van den Berg, A.; Olthuis, W.; Pascual-Garcia, C. Electrochemical Control of pH in Nanoliter Volumes. *Nano Lett.* **2018**, *18*, 2807–2815.
- (42) De, D.; Nicholson, P. S. Role of ionic depletion in deposition during electrophoretic deposition. *J. Am. Ceram. Soc.* **1999**, 82, 3031–3036.
- (43) Shilov, V. N.; Delgado, A. V.; Gonzalez-Caballero, F.; Grosse, C. Thin double layer theory of the wide-frequency range dielectric dispersion of suspensions of non-conducting spherical particles including surface conductivity of the stagnant layer. *Colloids Surf., A* **2001**. 192, 253–265.
- (44) Hashemi Amrei, S. M. H.; Miller, G. H.; Ristenpart, W. D. Asymmetric rectified electric fields between parallel electrodes: Numerical and scaling analyses. *Phys. Rev. E* **2019**, *99*, No. 062603.